Nanoparticle Geometry and Surface Orientation Influence Mode of Cellular Uptake

Heather Herd,[†,‡,§] Nicole Daum,[§] Arwyn T. Jones,[⊥] Hanno Huwer,[∥] Hamidreza Ghandehari,[†,‡,#,*] and Claus-Michael Lehr[§,△,*]

[†]Utah Center for Nanomedicine, Nano Institute of Utah, University of Utah, 36 S. Wasatch Drive, Salt Lake City, Utah 84112, United States , [‡]Department of Bioengineering, University of Utah, United States, [§]Helmholtz Centre for Infection Research, Helmholtz-Institute for Pharmaceutical Research Saarland, Saarland University, Campus, Building A4_1, D-66123 Saarbruecken, Germany, [⊥]Cardiff School of Pharmacy and Pharmaceutical Sciences, Cardiff University, Cardiff Wales, CF10 3NB, United Kingdom, [∥]Cardiothoracic Surgery, Heart Center Voelklingen, Germany, [#]Department of Pharmaceutics and Pharmaceutical Chemistry, University of Utah, United States, and [△]Biopharmaceutics and Pharmaceutical Technology, Saarland University, Campus, Building A4_1, D-66123 Saarbruecken, Germany

ABSTRACT In order to engineer safer nanomaterials, there is a need to understand, systematically evaluate, and develop constructs with appropriate cellular uptake and intracellular fates. The overall goal of this project is to determine the uptake patterns of silica nanoparticle geometries in model cells, in order to aid in the identification of the role of geometry on cellular uptake and transport. In our experiments we observed a significant difference in the viability of two phenotypes of primary macrophages; immortalized macrophages exhibited similar patterns. However, both primary and immortalized epithelial cells did not exhibit toxicity profiles. Interestingly uptake of these geometries in all cell lines exhibited very different time-dependent patterns. A screening of a series of chemical inhibitors of endocytosis was performed to isolate the uptake mechanisms of the different particles. The results show that all geometries exhibit very different uptake profiles and that this may be due to the orientation of the nanoparticles when they interact with the cell surface. Additionally, evidence suggests that these uptake patterns initialize different downstream cellular pathways, dependent on cell type and phenotype.

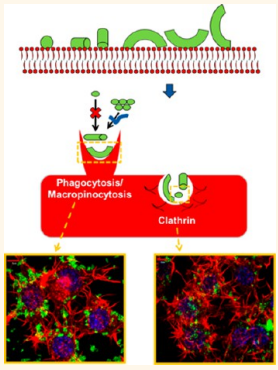

KEYWORDS: silica nanoparticle · nanotoxicity · endocytosis · cellular uptake · intracellular fate

The biomedical and engineering world has seen a drastic increase in the use of nanomaterials for therapeutic and diagnostic applications. However, it remains uncertain how nanomaterials interact with biological interfaces such as the plasma membrane of cells. Studies suggest that small alterations in physicochemical characteristics can drastically influence interactions of nanoparticles with the biological environment, affecting the mechanisms of cellular uptake and ultimately intracellular fate.[1,2] These changing interactions may also produce unintentional adverse effects, such as the induction of chronic inflammatory cascades. In order to engineer safe, efficient drug delivery systems, there is a need to develop a higher level of understanding of the mechanisms of uptake and intracellular fate of these constructs. Identification and systematic evaluation of the cellular uptake of nanomaterials will afford the development of target-specific constructs that deliver through a defined entry pathway leading to an appropriate intracellular fate with resultant bioactivity of the associated pharmacologically active ingredient.

It is generally appreciated that vesicular processes occurring at the cell membrane represent the prevailing route of uptake for these systems. For example, the accumulation of localized lipid raft domains induced by cell membrane interactions can be responsible for local membrane invaginations, facilitating nanoparticle uptake. Numerous endocytic routes exist, and some require activation *via* cell surface interactions to mediate receptor-mediated internalization.[3,4] For example, when conjugated to small nanoparticles, platelet endothelial cell adhesion molecule 1 (PECAM-1) and intercellular adhesion molecule 1 (ICAM-1) demonstrated increased uptake and transfection when compared to unconjugated ligand and large nanoparticle attachment.[5,6] However mechanisms such as

* Address correspondence to (H.G.) hamid.ghandehari@pharm.utah.edu; (C.M.L.) lehr@mx.uni-saarland.de.

Received for review August 12, 2012 and accepted February 12, 2013.

Published online February 12, 2013
10.1021/nn304439f

macropinocytosis and phagocytosis are nonspecific internalization modalities utilizing membrane ruffling to engulf nanoparticulates. Generally macropinocytosis and phagocytosis require membrane ruffling with actin polymerization, leading to enclosure of fluid or a physical entity such as a bacterium or particle.[7] It has been previously shown that shape modulates phagocytic potential, where the flexibility and curvature of a particle and cell membrane dictate the capability for internalization.[8] Endocytosis however is not always the only mechanism of internalization, as membrane association of nanoparticles can induce physical interactions that allow particle internalization, such as that observed with highly cationic dendrimer lipid bilayer disruption, which is hypothesized to induce transient cell holes and needle-like materials that stab membranes for internalization.[9,10] In general there is little consensus in the literature as to what uptake mechanism is used by most nanoparticles, a product of the limited availability of appropriate techniques to characterize internalization and diverse nanoconstructs. Recent literature suggests that alterations in characteristics of nanomaterials such as the radius of curvature, surface functionalization, size, geometry, and charge, can drastically affect uptake mechanisms and the intracellular fate of nanoparticles.[11−16] Investigations showed that highly positively charged polyplexes associated with negatively charged cell surface heparan sulfate proteoglycans, for example, were essential for inducing phagocytic-like mechanisms to internalize these constructs.[11] Additionally, geometric variations in silica nanoconstructs facilitated different levels of macropinocytosis uptake due to differences in cell surface GTPase interactions.[12] Small nanoparticle systems were shown to have reduced rates of uptake and variations in mechanisms of uptake with variations in surface properties. The authors suggested these slight changes significantly altered the protein corona and thus mechanistic internalization.[17] Mathematical analyses and experimental confirmations have been done to show that clathrin-mediated invaginations are due to elastic deformation of the membrane dependent on a critical nanoconstruct radius that provides essential energy minimization.[13,14,18] It is hypothesized that when a particle has a radius above this critical value, the cell membrane is unable to invaginate the particle,[13,14] facilitating a decrease in clathrin-mediated mechanisms. Additionally, evidence suggests that spherical particles with a size range around 200 nm or less are internalized *via* clathrin-mediated endocytosis.[15] Gratton *et al.* have suggested that cationic polymeric PRINT particles exhibited a high degree of uptake *via* macropinocytic and clathrin-mediated mechanisms, with a kinetic increase in rod-like particle uptake.[19,20] Other groups have shown geometric-dependent kinetic uptake, surface orientation, and toll-like receptor 2 upregulation, which enhanced the uptake of nonspherical particles.[21−23] Additionally, the unique orientation of rod-like nanoparticles into vesicular compartments in the perinuclear region has also been demonstrated, when compared to their spherical counterparts.[24] This evidence suggests that orientation of materials due to differences in geometry results in entering cells through separate mechanisms, which may potentially dictate the ultimate fate of the particles intracellularly.

The objectives of this study were to determine the uptake patterns of three different silica nanoparticle geometries, namely, spheres, cylinders, and worms, in model cells. These translationally relevant cell models were primary human alveolar macrophages, primary human tissue macrophages, primary human alveolar epithelial cells, immortalized RAW 264.7 mouse macrophages, and A549 human lung tumor epithelial cells. The cells were used to aid in the identification of the role of geometry on cellular uptake and intracellular transport. Our findings reveal that geometry plays a role in the defined mechanism of intracellular uptake and may potentially lead to a specified intracellular fate.

RESULTS AND DISCUSSION

Silica Nanoparticle Synthesis and Characterization. Three silica nanoparticle constructs were synthesized and characterized, as previously described:[25] worm-like, cylindrical, and spherical. Each construct was created such that charge, one dimension, fluorescence, and polydispersity were held constant (Supplemental Table 1 and Supplemental Figure 1). Polydispersity and the dimensions of the constructs were determined by the adjustment of the surfactant concentration while holding the stirring rate and heating of the solution constant. Charge and fluorescence attachment were determined by altering the ratio of surface modification to the number of particles in the solution.

Vialight Assay, Relative Nanoparticle Toxicity, and Cellular Uptake. To assess relative toxicity of the nanoparticles, cell viability at different concentrations was evaluated utilizing a measurement of the relative level of cellular adenosine triphosphate (ATP), an essential metabolic component in living cells. Relative nanoparticle cellular association and uptake was also assessed *via fluorescence-activated cell sorting* (FACS) and confirmed *via* confocal microscopy. No relative toxicity or nanoparticle uptake was observed in primary epithelial cells even at the highest concentration studied, and similar results were observed with the cell line A549 (Figure 1b and d, Supplement Figures 2d−f, 3b, and 4b and d). These results are corroborated with our previous findings that limited to no toxicity in epithelial cells following silica nanoparticle treatment was observed.[26] Additionally, these cells themselves serve primarily as a protective barrier and do not generally take up foreign material through phagocytic processes like

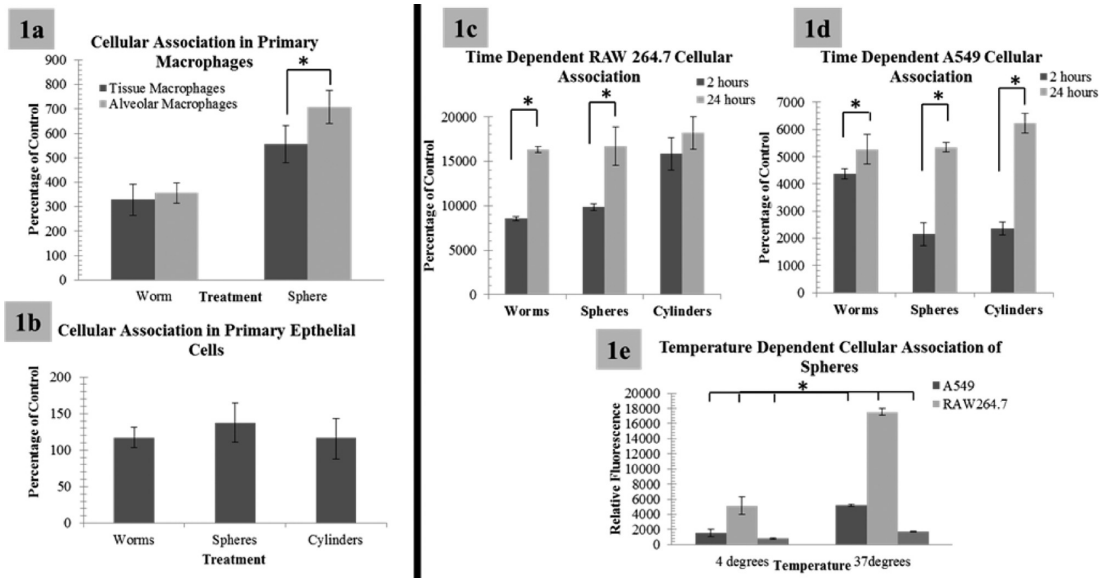

Figure 1. Basal uptake of geometrically defined nanoparticles. Relative uptake of 75 μg/mL of nanoparticles at specified time points assessed *via* FACS. (a) Macrophages exhibit significant uptake. However, both the phenotype of the macrophage and the geometry (at this time point, 1.5 h) appear to play important roles in the degree of uptake. It is also important to note that alveolar macrophages treated with spherical nanoparticles when compared to worm-like nanoparticles appear to have a greater degree of nanoparticle uptake, at this time point. This suggests a phenotypic and geometric implication. (b) Epithelial cells exhibit little to no nanoparticle uptake when compared to control. (c, d) Relative uptake of 75 μg/mL of nanoparticles at specified time points assessed *via* FACS. As shown, initial time point analysis shows a variation in the uptake rate of nanoparticles, dependent upon geometry, while later time points appear to have an equivalent rate of cellular association (for clarity some time points have been removed; please see Supplemental Figure 5 for all time points). (e) Representative graph of the relative uptake of spherical nanoparticles as a function of temperature in model cells. Alveolar macrophages are depicted by their increased uptake potential. The graph provides confirmation of energy-dependent mechanisms of uptake. Please note: graphs are represented as percentage of control or the background provided by FACS analysis of cells incubated without nanoparticles; so 100% would be 100% of control. Low levels of autofluorescence were indicated for immortalized lines, while high levels were indicated for primary cells due to donor variations including unknown patient treatment (chemotherapeutics, smoker or nonsmoker, other diseases/treatments, *etc.*) *Indicates statistical significance *p* value <0.05.

macrophages. Primary macrophages however were observed to follow a trend similar to RAW 264.7 cells (Figure 1a, Supplemental Figures 2−4), where high concentrations of nanoparticles exhibited toxicity (Supplemental Figure 4a and c) and a high degree of uptake (Figure 1a and c) was observed, while lower concentrations did not appear to exhibit a toxic effect. Interestingly, macrophage phenotypic variations did show differences in nanoparticle uptake (Figure 1a, Supplemental Figure 3a), suggesting that not only cell type but also cell phenotype have implications on toxicity and uptake of nanoparticles.

Time-Dependent Uptake. In an attempt to assess the relative mode of uptake of these geometries, a time point assay to determine the uptake saturation point was performed. During these experimental analyses it was observed that initially cells had variations in the rates of uptake that appeared to be dependent on the geometry of the nanoparticle, while at later time points, labeling became saturated and equilibrated to a level that was irrespective of geometry (Figure 1c and d, Supplemental Figure 5). These slight variations in the rates of uptake could potentially be due to differences in the internalization mechanisms of the nanoparticles, where some could be harnessing multiple or faster endocytic mechanisms.

Energy-Dependent Mechanisms of Uptake. To determine if mechanisms of uptake were due to endocytosis (or other energy-dependent mechanisms) or membrane association, cells were incubated at 4 and 37 °C to evaluate the relative level of particle internalization. This method provides a reduction in the relative energy-dependent processes within cell models, effectively eliminating endocytosis. It was observed that there was a greater degree of cellular association at 37 °C when compared to 4 °C, suggesting energy-dependent or endocytic mechanisms of uptake (Figure 1e and Supplemental Figure 6). It does appear that some amount of nanoparticle uptake occurs at 4 °C, suggesting that they could interact with the membrane of the cell and facilitate uptake independent of energy active processes. It is also conceivable that this fraction is associated with the plasma membrane and not internalized. It is important to note that a majority of this nonspecific uptake occurs in A549 cells, rather than RAW 264.7 cells, suggesting that it could be a cell-dependent phenomenon. Since the majority of uptake was energy dependent, we then proceeded to further investigate what endocytic processes the nanoparticles were using to gain access to the cells.

Mechanisms of Uptake. A preliminary screening of a series of inhibitors was performed to isolate the initial

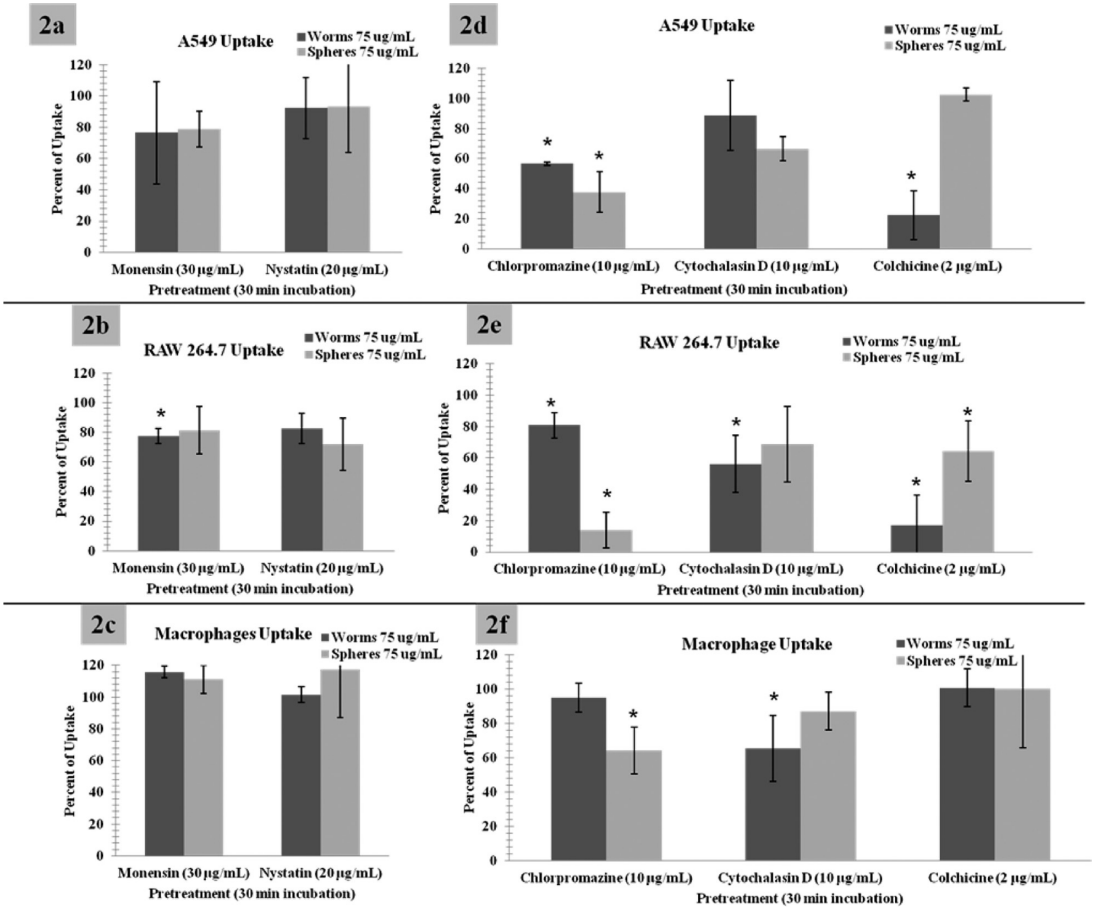

Figure 2. (a–c) Relative level of nanoparticle uptake when incubated with monensin (clathrin- and caveolin-independent endocytosis inhibitor) and nystatin (caveolin endocytosis inhibitor). This suggests that caveolin-mediated endocytosis is not involved in the internalization of these nanoparticle systems. (d–f) Cytochalasin D and colchicine are phagocytic and macropinocytosis inhibitors, while chlorpromazine inhibits clathrin-mediated mechanisms. The results show that there is a statistically significant reduction in nanoparticle uptake for these three inhibitors, but all geometries show very different uptake profiles. This suggests that the mechanisms by which these particles are entering the cells vary and are dependent on the relative shape (or size). For clarity and due to the significant similarities of worms and cylinders, cylindrical data have been moved to the Supporting Information. Please note: graphs are represented as percentage of uptake or the background provided by FACS analysis of cells incubated with spheres or worms without the respective inhibitor. *Indicates statistical significance from control p value <0.05. Macrophages are alveolar macrophages.

uptake mechanisms of the different particles. Nystatin was used to increase membrane fluidity *via* the depletion of cholesterol and reduce the formation of lipid caveolar rafts.[27] Monensin was used as an ionophore that facilitates an increased exchange of sodium ions and is generally considered an inhibitor of caveolae and clathrin-independent endocytosis.[28] Both of these inhibitors did not show a significant decrease in nanoparticle uptake (Figure 2a–c). This is a predictable result, as the nanoparticles are much larger in size than what is considered to be "normally" taken up by caveolae rafts.[29] It is important to note while epithelial cells normally express caveolae rafts, little is known about similar expression in macrophages. However, inflammatory phenotypes of macrophages including mouse macrophages and alveolar macrophages have been shown to express and in some cases overexpress caveolin.[30,31]

Three more inhibitors were involved in this initial screen, namely, cytochalasin D, colchicine, and chlorpromazine. Cytochalasin D and colchicine are phagocytic and macropinocytosis inhibitors. Cytochalasin D prevents actin polymerization, and colchicine inhibits microtubule polymerization, both of which reduce membrane ruffling.[32–34] Chlorpromazine reduces invaginations *via* clathrin-mediated endocytosis by depleting the plasma membrane of clathrin and adaptor proteins and sequestering them on intracellular vesicles. The results in Figure 2d–f show that there is a statistically significant reduction in nanoparticle uptake for these three inhibitors. However, all geometries show very different uptake profiles. Clathrin-mediated inhibitors appear to be reducing the amount of spherical uptake, while macropinocytosis and phagocytic inhibitors appear to be reducing worm-like nanoparticle uptake. These observations suggest that the mechanisms by which the particles are entering the cells vary and are dependent on their relative shape (or size). We did however detect some variations in observations,

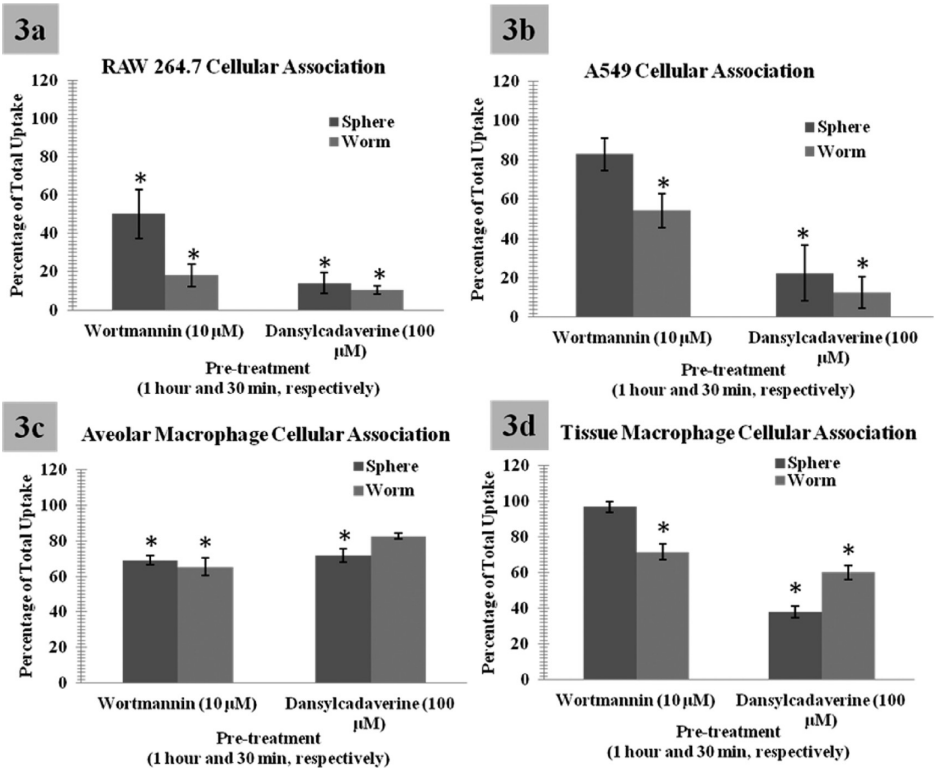

Figure 3. Flow cytometry analysis to quantitatively assess the uptake of nanoparticles. Due to low specificity in endocytic inhibitors, dansylcadaverine (a clathrin inhibitor) and wortmannin (a phagocytic and macropinocyotsis inhibitor) were utilized to confirm the apparent variations in uptake due to changes in geometry. As shown, dansylcadaverine blocks both sphere and worm uptake, but to a more significant degree spherical uptake. However, wortmannin is observed to block worm-like uptake to a more significant degree, supporting geometric variations in cellular uptake. Additionally, differences in uptake due to the cell phenotype were observed. For clarity and due to the significant similarities of worms and cylinders, cylindrical data hasve been moved to the Supporting Information. Please note: graphs are represented as percentage of uptake or the background provided by FACS analysis of cells incubated with spheres or worms without the respective inhibitor. *Indicates statistical significance from control p value <0.05.

as shown in Figure 2, where cytochalasin D did not exhibit the same degree of inhibition as colchicines induced, suggesting that microtubules may play a more important role in the polymerization pathways responsible for the extravasations. It is interesting to note that similar results with colloidal gold have been observed previously.[35]

Due to this variability, and because endocytic inhibitors can induce toxicity (Supplemental Figure 7) and lack specificity and efficacy,[11] dansylcadaverine and wortmannin were utilized to confirm the apparent variations in uptake due to differences in geometry. Dansylcadaverine treatment blocked the formation of coated pits by inhibiting transglutaminase in the cell membrane, which will reduce receptor-mediated endocytosis (clathrin mediated).[36] Wortmannin prevents fluid phase endocytosis (macropinocytosis) by inhibiting multiple isoforms of PI 3-kinase (phosphatidyl inositol-3-kinases).[32] As shown in Figure 3 dansylcadaverine blocked both sphere and worm uptake. Wortmannin blocked worm uptake to a greater extent. Additionally, to some degree both cell type and phenotypic differences were observed. Confocal image analysis confirmed all FACS results within all pharmacological screens (data not shown). Two concentrations of wortmannin were tested, in an attempt to discern between macropinocytosis and phagocytic uptake;[37,38] however neither showed significant difference from one another (Supplemental Figure 8).

These pharmacological inhibitor results are indicative of geometrically specific mechanism(s) of uptake, primarily clathrin-mediated endocytosis for spherical particles and macropinocytosis or phagocytosis for worm particles. It is hypothesized that this phenomena is due to the orientation of the nanoparticles when they interact with the cell surface (Figure 4) and that geometry provides a unique advantage because alteration in this parameter allows for the design of multiple approach mechanisms. For example, a spherical nanoparticle has only one face that can interact with the cell surface, while cylindrical and worm-like nanoparticles have multiple faces with large variations in size in each dimension. If one draws a correlation between the physicochemical characteristics (or dimensions) of these nanoparticles and endocytic mechanisms, one can identify or predict their primary mode of uptake (Figure 4). For example spheres have one dimension of approximately 200 nm, which may be expected to be

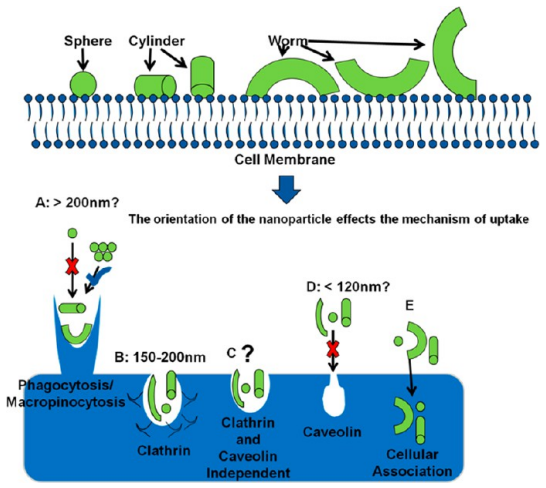

Figure 4. Cartoon depicting the hypothesis that the orientation of the nanoparticle influences the mechanism of uptake. (A) Macropinocytosis has been shown to occur at the microscale, fitting with one dimension of cylinders and worms. However, spheres, unless aggregated, do not fit this criterion. (B) Theoretically if oriented properly, all particles could be taken up *via* clathrin-mediated mechanisms. (C, E) Other mechanisms of uptake not readily identifiable are plausible. (D) Caveolin-mediated invaginations are theoretically much too small for the nanoparticle size range tested here.[29]

within the size range of clathrin-mediated endocytosis. It is important however to note that this dimension is on the larger end of normal clathrin invaginations.[39] This dimension however is too large for caveolin-mediated endocyotsis and too small for phagocytosis unless the spheres are aggregated. However, evidence does suggest that macropinocytosis can occur in small size ranges.[7] Thus, it is hypothesized that clathrin-mediated endocytosis is the primary mechanism of uptake for the spherical nanoparticle systems. Worms and cylinders however had one dimension of approximately 200 nm, within the clathrin limits, and another dimension (~400 and 1300 nm) that was within the limits of macropinocytosis and phagocytosis. Thus, it is possible that both the end of the particle and the longitudinal rotation of the particle could interact with the cell surface, effectively harnessing both mechanisms of uptake. It is more probable that macropinocytosis and or phagocytosis are the mechanisms of uptake of these particles due to their relatively large size. Additionally, when comparing the transversal (small) axis of the nanoparticle to the longitudinal axis, it is more likely that the longitudinal axis will have a higher positive charge. Thus, it is more probable that there will be an axial rotational association of the particle with the net negative charge of the cell membrane, leading to an energy maximum. Similar observations were made previously for microparticles at the nucleus and surface.[24,40,41]

Dextran and Transferrin Co-localization. To further confirm uptake pathways, we utilized traditional markers for co-localization. Transferrin is a well-characterized marker of clathrin-mediated uptake, and dextran is primarily used as a marker for fluid phase uptake and macropinocytosis.[39] As observed in the pharmacological inhibition experiments, a greater degree of transferrin co-localization was observed with spherical nanoparticles, while colocalization with dextran appears to be equivalent (Figure 5A and C, transferrin and dextran, respectively) when compared to worm-like nanoparticles (Figure 5B and D, transferrin and dextran, respectively) in both RAW 264.7 and A549 cells. It is important to note however that in both cases co-localization did occur in the worm-like nanoparticle conditions, suggesting that clathrin- and fluid-phase-mediated mechanisms may both play a role in the uptake of these particles.

Actin Polymerization. To provide further visual evidence of endocytosis and to prove the involvement of actin polymerization mechanisms, a phalloidin stain was used to label the cell lines studied. As observed in Figure 6, A and D, spherical and worm nanoparticle treatment, respectively, have very different actin polymerization patterns. The apparent actin polymerization patterns include polymerization into bowl-like structures just below the surface of the cell (B, C, E, and F) and extravasations polymerizing above the surface of the cell. Both of these patterns appear to be associated with the nanomaterials. The polymerization patterns could be suggestive of the involvement of clathrin-mediated, macropinocytic, and phagocytic mechanisms.

Transmission Electron Microscopy of Endocytosis. From experiments with labeled actin showing the involvement of surface protrusions we performed further ultrastructural analysis of cells incubated with these nanoparticles. Here, following 15 min of incubation with worm and spherical nanoparticles, cells were imaged *via* TEM. Visualization suggests that worm-like particles were mostly associated with extravasations from the membrane (Figure 7E and G), as well as particle wrapping like protrusions (Figure 7F). Invaginations where spherical particles seemed to be associated with the cellular membrane were observed (Figure 7A and B). Particles were also observed in the intracellular space within 15 min (Figure 7G for worms and C for spheres), an unusually rapid internalization for nanoparticle systems. Additionally, several nanoparticles appear to be clumped, suggesting that particles are entering through similar pathways or being sequestered by the cell. It is important to note that spherical particles appear to be internalized and associate with the plasma membrane much more rapidly than worm particles. More particles reside within the intracellular space and around the membrane within that time frame, correlating with the time-dependent FACS cellular uptake results. However, as observed previously, nanoparticle content does reach an equivalence at later time points.[25] This suggests that spherical

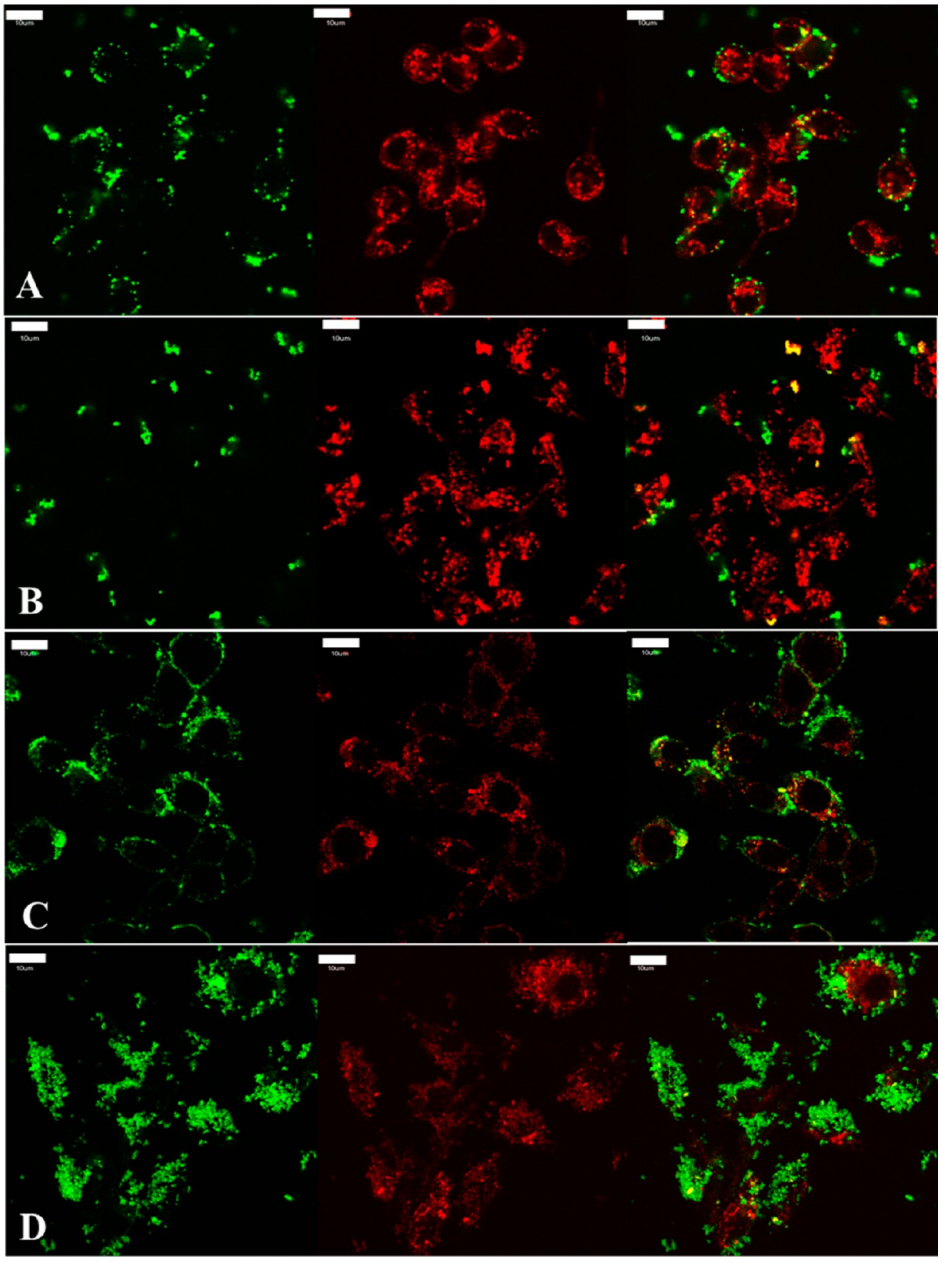

Figure 5. Transferrin and dextran, intracellular markers of clathrin-mediated endocytosis and fluid phase endocytosis, respectively, were co-incubated with silica nanoparticles to investigate the degree of co-localization to confirm clathrin- and fluid-phase-mediated mechanisms; RAW 264.7 cells shown. (A, B) A single focal plane and the respective channels of live cells after 15 min of incubation. Transferrin is labeled in red, nanoparticles are labeled in green (A is spherical treatment and B is worm-like treatment, both at 75 μg/mL), and the co-localization is depicted in yellow between particles and transferrin. (C, D) Fluorescence from all Z stacks and respective channels of fixed cells after 30 min of incubation. Dextran is labeled in red, particles are labeled in green (C is spherical treatment and D is worm-like treatment at 75 μg/mL), and yellow represents the co-localization between nanoparticles and dextran. There appears to be a higher degree of co-localization of both these cellular internalization markers with spherical nanoparticles when compared to worm-like nanoparticles, suggesting that a higher degree of clathrin- and fluid-phase-mediated endocytosis occurs with these systems. It is important to note that the co-localization (yellow) in all images suggests that clathrin- and fluid-phase-mediated endocytosis is at play for all geometries tested. For clarity and due to the significant similarities of worms and cylinders, cylindrical data have been moved to the Supporting Information. Scale bars: 10 μm.

particles are internalized more rapidly, due to either their relative size or the internalization mechanism. Worm-like particles and spherical particles are completely internalized at 24 h, as depicted in Figure 7D and H.[25] These sequestering mechanisms appear to continue at 24 h.

PI 3-Kinase Pathway Upregulation after Nanoparticle Uptake. In an attempt to begin to understand the cues behind this sequestering mechanism, initial gene expression levels were analyzed after a 1.5 h incubation period with nanoparticles. As briefly introduced earlier, PI 3-kinase is an essential protein in the formation and

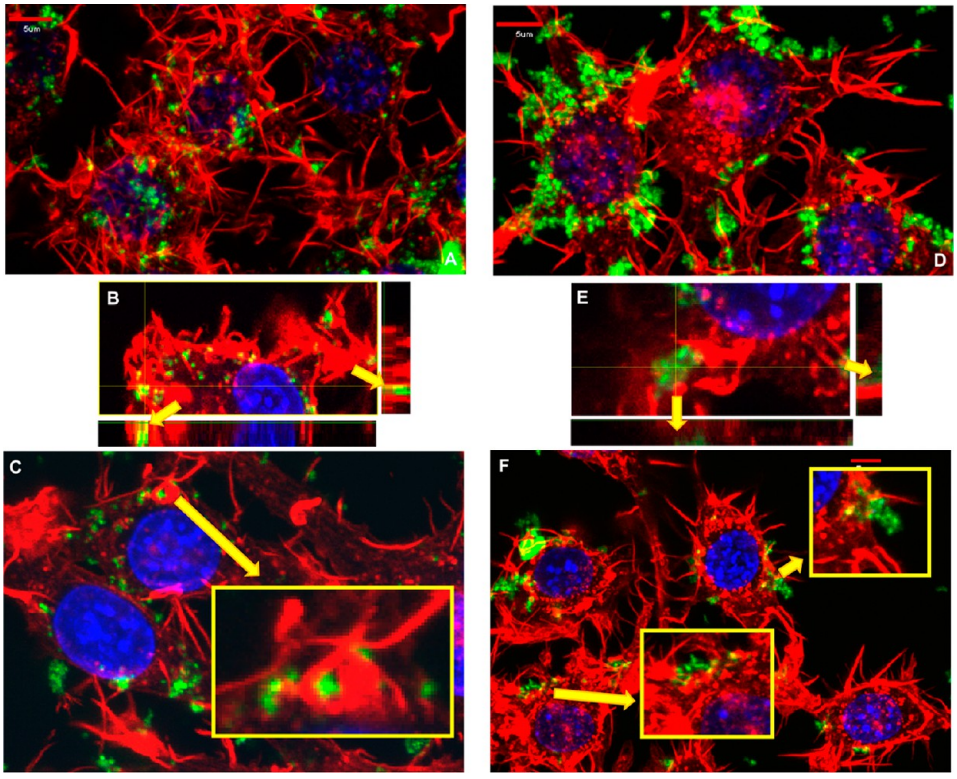

Figure 6. Actin polymerization staining in RAW 264.7 cells, involved in mechanisms of endocytosis, is depicted to visualize the hallmark endocytic process involved in the internalization of these particles. Red: phalloidin stain of actin polymerization, green: nanoparticle FITC attachment, and blue: DAPI nucleus stain. (A–C) Spherical nanoparticle and (D–F) worm nanoparticle treatment after 15 min. Spherical nanoparticle treatment (A) and worm nanoparticle treatment (D) appear to induce very different polymerization patterns. The polymerization patterns observed in treated cells include invaginations within the membrane associated with nanomaterials, identified in the zoomed inset in C and in the depiction of the Z stack in B, while other polymerization patterns appear to be extravasations from the membrane associated with nanomaterials, marked in the zoomed insets in F and the Z stack in E. These polymerization patterns could suggest the involvement of clathrin-mediated, macropinocytic, and phagocytic mechanisms. For clarity and due to the significant similarities of worms and cylinders, cylindrical data have been moved to the Supporting Information.

budding of macropinosomes in the intracellular environment,[38] and our results indicated that PI 3-kinase inhibition with wortmannin facilitated a reduction in the nanoparticle uptake and potentially the formation of macropinosomes in tissue macrophages (Figure 3). This led us to believe that downstream gene expression levels within the PI 3-kinase pathway could potentially provide insights into how cells cope with the intracellular uptake of these nanoparticles. Thus, following the incubation period, the RNA from tissue and alveolar macrophages was isolated and subjected to a PI 3-kinase signaling PCR array from SABiosciences (Qiagen, Valencia, CA, USA). This array is complete with 84 genes that are either directly or closely related to this signaling cascade and could potentially provide some additional insight into genes that might cause downstream intracellular signaling and ultimate intracellular fate. While all treatments caused a regulation of these genes, a greater degree of regulation was observed with worm-like treatments when compared to spherical treatments (Figure 8). This suggests that PI 3-kinase may potentially be affected to a greater degree in worm-like treatments when compared to spherical counterparts; however all nanoparticle treatments may induce this cascade. It is important to note that there is a significant difference between the affects in tissue and alveolar macrophages, suggesting that tissue macrophages might have an increased fluid phase or macropinocytic function. Or alternatively an increase in phagocytic activity could be present in alveolar cells due to their native physiological function, which may operate independently of PI 3-kinase.

The regulated genes were further processed *via* data mining bioinformatics online freeware services (GATHER)[42] to identify other pathways that could potentially be responsible for the observed regulation. It was seen that a majority of the genes were interconnected and regulated cell size and growth, phosphorylation, focal adhesion, cell signaling, cell surface receptors, toll-like receptor signaling, insulin signaling, and ribosomal protein S6 kinases (Supplemental Table 2).

In our previous observations, cells appeared to take up and eventually sequester a certain concentration of nanoparticles in autophagic compartments. Below this threshold the cells were able to proliferate and function "normally", while above it they underwent what

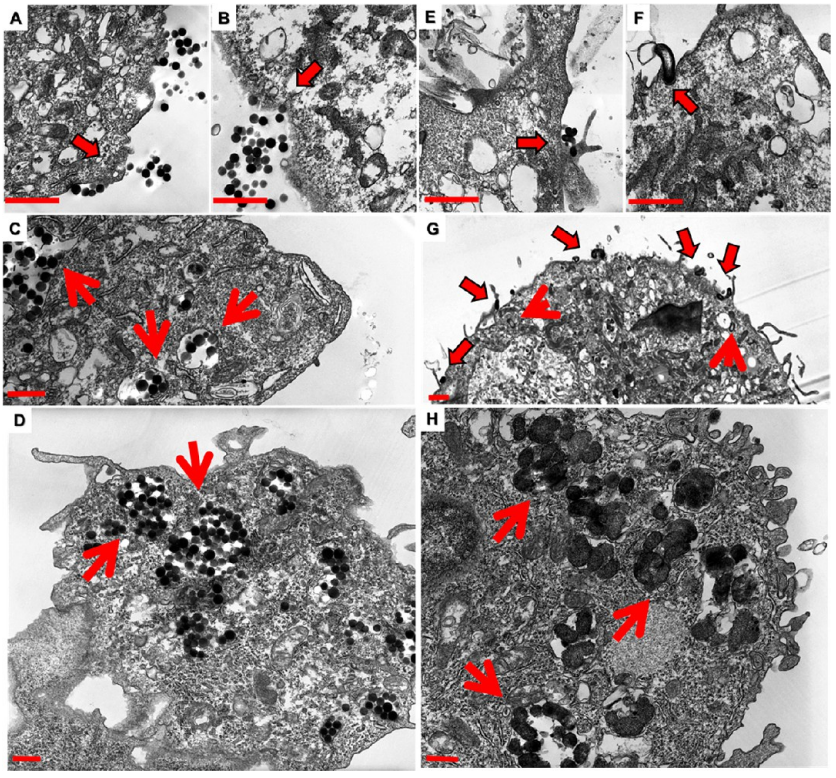

Figure 7. Following 15 min of incubation with both worm and spherical nanoparticles, cells were fixed and imaged *via* TEM. Membrane invaginations are associated with spherical particles (A and B). Membrane extravasations however are observed to be associated with worm particles (E and G), and membrane wrapping associated with worm-like particles (F and G) is observed. Both nanoparticles are observed within the cytoplasm of these cells at 15 min (C and G), while there is a greater degree of uptake of spherical nanoparticles at this time point. This suggests that spherical particles are taken up more rapidly than worm nanoparticles. However, a greater amount of both nanoparticles is internalized at 24 h time points, as we observed previously (D and H).[25] Additionally, there appears to be some type of sequestering mechanism at play. For clarity and due to the significant similarities of worms and cylinders, cylindrical data have been moved to the Supporting Information. Scale bars: 1 μm.

appeared to be necrotic cell death.[25] This threshold mechanism appeared to be independent of geometric variations at a 24 h time point.[25] Using similar nanoparticles, in this study we observed that variations in the mechanisms of and the accumulation rate of uptake are dependent on the geometry. Yet, at later time points, we still observe a threshold mechanism in both immortalized and primary cells.

If we connect this gene expression to our previous findings, we might be able to link the initial gene expression to the ultimate intracellular fate of these nanoparticles. In our PCR analysis we identified the presence of cell size and growth, phosphorylation, focal adhesion, cell signaling, cell surface receptors, and toll-like receptor signaling gene regulation pathways (Supplemental Table 2). However we also identified the involvement of insulin signaling and ribosomal protein S6 kinase pathways (Supplemental Table 2). While it is expected that the former signaling cascades would be induced due to local interactions of the nanoparticles with the cell surface, the latter seems surprising. One would expect that with an increase in macropinocytosis activity one would see an increase in the relative cell size, leading to an increase in the amount of material that could be taken up by the cells. Additionally, focal adhesions might need to be initiated to induce cellular internalization and surface receptors would be initiated with nanoparticle interactions. However, the latter two signaling cascades are surprising. Yet, if one takes a look at previously reported data, it can be seen that nanoparticles including silica nanoparticles[25] have been implicated in an intracellular trafficking and signaling event called autophagy. Not only does PI 3-kinase signaling play an important role in the initiation of these events, but so do the insulin and ribosomal protein S6 kinase signaling cascades.[43−45] The potential implication of these cascades could suggest that internalization is inducing intracellular signaling gene cascades, leading to ultimate intracellular fate or sequestering within autophagic compartments.

If intracellular fate is determined upon cellular internalization, it means that the manipulation of these uptake patterns could provide enhanced specific delivery properties. Thus, it will be important in further research to identify specific patterns in the biological response in both protein and gene

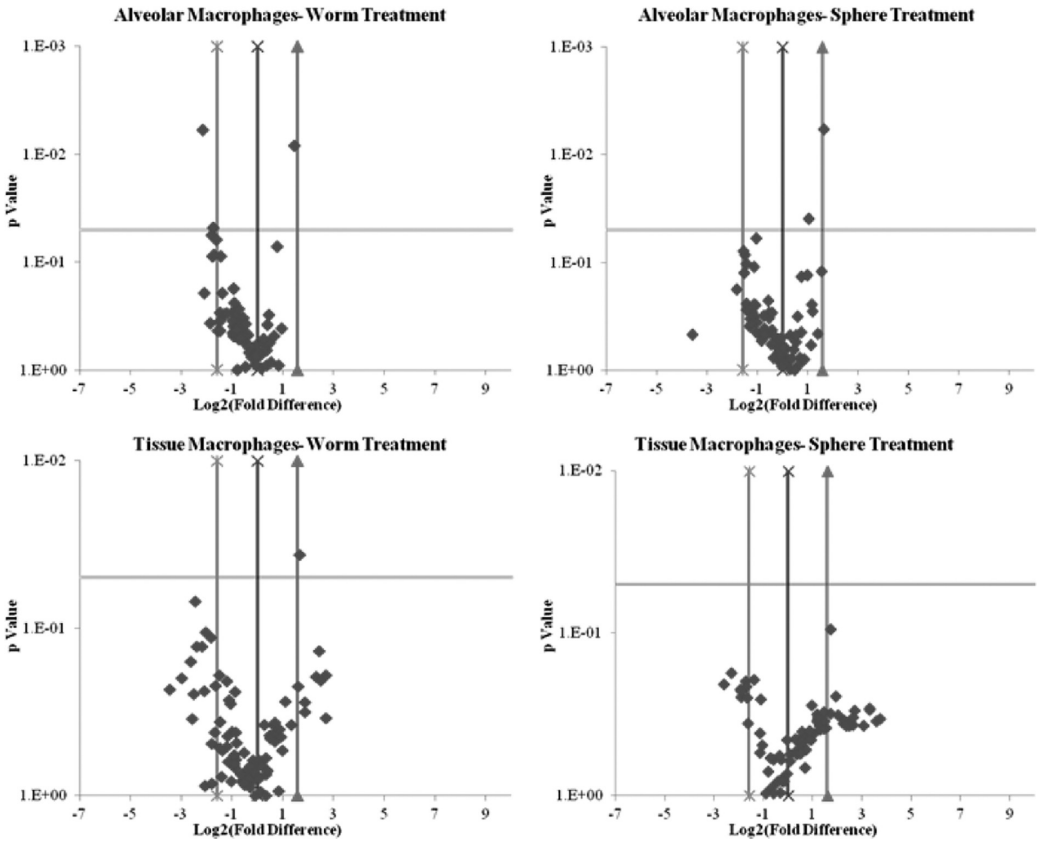

Figure 8. PI 3-kinase array analysis volcano plots of primary macrophages regulated genes. More regulation is observed in tissue macrophages when compared to alveolar macrophages, suggesting a different pattern of uptake due to phenotypic differences. This could also potentially play an important role in toxicity. Additionally, worms regulate genes to a more significant extent than spheres do in both tissue and alveolar macrophages. However, it is plausible that particle treatment itself could induce this regulation.

expression and correlate that to the physicochemical characteristics.

CONCLUSIONS

In summary, in this report we have shown that geometry plays an important role in the uptake of nanoparticles. Nanoparticle uptake was induced *via* a variety of different endocytic and cellular association mechanisms, dependent on the geometry. Within this size range with highly positively charged materials, it appears that clathrin-mediated endocytosis was the primary mechanism of uptake for spherical particles, while those materials with a larger dimension appear to be taken up primarily through macropinocytosis or phagocytic mechanisms. However, all materials to some degree were taken up *via* both mechanisms. Additionally, we have shown that phenotypic differences within cell types can lead to very different uptake profiles, suggesting that cell function plays an important role in nanoparticle toxicity.

EXPERIMENTAL METHODS

Silica Nanoparticle Synthesis and Characterization. Silica nanoparticles were synthesized and characterized as described previously.[25] Briefly porous silica nanoworms, -spheres, and -cylinders were synthesized utilizing modified Stober methods.[3,46] 3-Aminopropyltriethoxysilane was coupled to the surface of the silica nanoparticles by procedures described earlier.[47] All particles were fluorescently labeled with fluorescein isothiocyanate (FITC) to assess cellular uptake (~2.9, 3.5, and 6.5 mg of FITC per 100 mg of worms, cylinders, and spheres, respectively). The constructs were sterilized by dry autoclavation. Following synthesis the size and shape of the particles were determined by transmission electron microscopy (TEM). Zeta potential of the constructs was measured using a Malvern Instruments Zetasizer Nano ZS. The absence of cetyltrimethylammonium bromide and presence of primary amine after acid hydrolysis was ascertained by infrared spectroscopy and thermogravimetric analysis.

Cell Culture. Human adenocarcinoma alveolar basal epithelial A549 cells and RAW 264.7 murine macrophages were obtained from ATCC (Manassas, VA, USA) and maintained in the recommended media supplemented with 10% FBS. Cell cultures were incubated at 37 °C in 5% CO_2 and 95% humidified air and kept in logarithmic phase of growth throughout all experiments. In general, cells were seeded at ~15 000 cells per cm^2.

Primary epithelial cells and macrophages were isolated and cultivated, as described previously.[48,49] Briefly, human lung tissue was obtained from patients undergoing lung resections. The tissue was sliced and washed repeatedly with a balanced

salt solution. The tissue slices were collected, pelleted, and incubated with hypotonic buffer to isolate alveolar macrophages. The remaining tissue slices were digested with a trypsin−elastase combination and filtered prior to an incubation of the resulting fluid in a Petri dish for 90 min to allow for tissue macrophage attachment. Unattached cells in the Petri dish underwent a Percoll density gradient and cell sorting with magnetic beads to isolate purified human alveolar epithelial type II cells. Both macrophages and epithelial cells were seeded at 500 000 cells in a 12-well plate. Macrophages were cultivated in MΦ medium (RPMI 1640, 5% FCS, 100 U/mL penicillin G, 100 μg/mL streptomycin, 2 mM glutamine) for 4−5 days to ensure appropriate receptor expression. Epithelial cells were cultivated in SAGM small airway epithelial cell growth medium (SAGM Airway Bullet Kit, CC-3118), with supplements including bovine pituitary extract, hydrocortisone, human epidermal growth factor, epinephrine, insulin, triiodothyronine, transferrin, gentamicin/amphotericin B, retinoic acid, and BSA-FAF (Lonza, Verviers, Belgium) supplemented with penicillin (100 units/mL), streptomycin (100 μg/mL), and 1% fetal calf serum and were maintained for 10 days until confluence. All cultures were kept at 37 °C in a 5% CO_2 humidified atmosphere.

Measurement of Cell Viability. Cells were exposed to a range of concentrations (30−500 μg/mL) of silica nanoparticles for 2 and 24 h. They were subsequently washed with phosphate buffer saline (PBS), and relative cell viability was assessed by utilizing a luciferase enzyme, which is converted to a bioluminescent molecule *via* ATP, a required element in living cells. The luciferase enzyme is the key component in the Vialight Assay (Lonza,Verviers, Belgium), and assessment of relative cell viability was obtained using manufacturer's protocols. Light intensity measurements were performed using an Infinite M200 microplate reader (Tecan, Crailsheim, Germany). IC_{50} values were calculated utilizing GraphPad Prism software (La Jolla, CA, USA).

Cellular Uptake Visualization, Quantification, and Time Point Analysis. The uptake of silica nanoparticles by cultured cells was visualized by confocal microscopy. Cells were grown on 24-well imaging plates at a density of ∼9000 cells/cm^2 and incubated for 24 h with 75 μg/mL FITC-labeled silica nanoconstructs. After incubation, cell membranes were stained with rhodamine-labeled wheat germ agglutinin (rhodamine-WGA) and fixed with 4% formalin in PBS. Cell nuclei were stained with 2.5 μM 4′,6-diamidino-2-phenylindole (DAPI) according to the manufacturer's protocol. Fluorescent images of fixed cells were taken under a confocal laser scanning microscope (LSM510; Zeiss, Jena, Germany). The intensity of the laser beam and the photodetector sensitivity were kept constant in order to compare the relative fluorescence intensities between experiments. Z stacks were collected and localization was assessed utilizing the LSM510 software package. 3D reconstruction, visualization of intracellular particles, image acquisitions, and analyses were performed using Velocity (Improvisions, Lexington, MA, USA).

Flow cytometry analysis was used to quantify the amount of nanoparticle uptake. Cells were grown on 12-well plates at a density of ∼15 000 cells/cm^2 and incubated with 75 μg/mL FITC-labeled silica nanoconstructs for various time points (0.5, 1, 2, 4, 6, 12, and 24 h). Following incubation, cells were trypsinized (epithelial cells) or scraped (macrophage cells) to obtain a single-cell suspension. Cells were suspended in PBS containing 1% BSA, and analysis was performed on a FACSCalibur (BD Biosciences, Heidelberg, Germany). Emitted light resulting from FITC-labeled nanoparticles was detected by the FL-2 detector. To calculate the background fluorescence of unlabeled cells, cells without any addition of nanoparticles were carried along as a negative control in every measurement. For whole-cell analysis 10 000 cells were counted. Data analysis was performed with BD CellQuest Pro (BD Biosciences, Heidelberg, Germany).

Energy-Dependent Mechanisms. Flow cytometry analysis was used to quantify the amount of nanoparticle uptake. Cells were grown on 12-well plates at a density of ∼15 000 cells/cm^2 and incubated with 75 μg/mL FITC-labeled silica nanoconstructs for 2 h at 4 and 37 °C. Analysis and quantification methods were identical to quantification and time point analyses.

Studies with Chemical Inhibitors of Endocytosis. The relative level of nanoparticle uptake was assessed *via* confocal microscopy and flow cytometry. Cells were grown on 24-well imaging and 12-well cell culture plates (confocal and FACS, respectively) at a density of ∼15 000 cells/cm^2. They were preincubated with endocytosis inhibitors prior to a 1.5 h incubation with 75 μg/mL FITC-labeled silica nanoconstructs. Following incubation, confocal and FACS analysis (as outlined previously) were performed. Nanoparticle-only treated cells were utilized as positive controls and compared to inhibitor plus nanoparticle-treated cells. Caveolin-dependent endocytosis was assessed utilizing nystatin at a 30 min preincubation at 20 μg/mL. Clathrin-dependent endocytosis was assessed utilizing a 30 min preincubation with either 100 μM dansylcadaverine or 10 μg/mL chlorpromazine. Clathrin- and caveolin-independent endocytosis were assessed utilizing a 30 min pretreatment with 30 μg/mL monensin. Phagocytosis and macropinocytosis were assessed utilizing a single inhibitor; the following were used: 1 h incubation with 10 μM or 10 nM concentrations of Wortmannin or a 30 min preincubation with 10 μg/mL cytochalasin D or 2 μg/mL of colchicine. Concentrations were obtained from reported literature values.[50,51] Cell viability was tested for all concentrations of each inhibitor after 3 h of incubation.

Dextran and Transferrin Co-localization. The co-localization of silica nanoparticles with Alexa Fluor 633-labeled dextran and transferrin (Invitrogen Corp., Carlsbad, CA, USA) by cultured cells was assessed by confocal microscopy. Cells were grown on 35 mm glass bottom microwell dishes at a density of ∼9000 cells/cm^2 (MatTek, Ashland, MA, USA) and incubated with either a 15 min co-incubation with 75 μg/mL FITC-labeled silica nanoconstructs and Alex Fluor 633-labeled transferrin or 30 min with 75 μg/mL FITC-labeled silica nanoconstructs and 50 μg/mL Alex Fluor 633-labeled dextran. Fluorescent images of fixed cells were taken by CLSM as described above.

Actin Labeling with Rhodamine Phalloidin. To assess the relative proximity of silica nanoparticles to polymerized actin, following fixation cells were assessed *via* confocal microscopy. First, cells were grown on 35 mm glass bottom microwell dishes at a density of ∼9000 cells/cm^2 (MatTek, Ashland, MA, USA) and incubated for 15 min with 75 μg/mL FITC-labeled silica nanoconstructs. Following incubation with the nanoparticles the actin cytoskeleton was labeled essentially according to the manufacturer's instructions. Briefly cells were washed with PBS, fixed with 3.7% formaldehyde solution for 10 min, washed with PBS, and permeabilized by 0.1% Triton X-100 in PBS. The cells were then washed with PBS and incubated for 20 min with 5 μL of rhodamine phalloidin from a 200 units/mL methanolic stock. Cells were washed a final time, fixed, and mounted for CLSM imaging.

Transmission Electron Microscopy. The uptake of silica constructs by cultured cells was assessed by transmission electron microscopy. Cells were seeded on six-well plates containing 1 × 1 cm ACLAR plastic at 2 × 10^5 cells per well. After an overnight incubation, 50 μg/mL of silica nanoconstructs was added, and cells were incubated for 15 min, after which they were washed with PBS and fixed with a 2.5% glutaraldehyde and 1% formaldehyde in 0.1 M sodium cacodylate buffer with sucrose and calcium chloride. Cells were stained with uranyl acetate for 45 min at room temperature, and TEM images were taken with a Phillips TECHAI F2 TEM (Hillsboro, OR, USA) at an accelerating voltage of 80 kV.

Real-Time PI3K-AKT Signaling PCR Array. RNA was isolated from three separate patient samples of primary alveolar and tissue macrophages using an RNeasy Mini Kit (Qiagen), and genomic DNA was removed utilizing an RNase-Free DNase Set (Qiagen, Valencia, CA, USA). Total RNA was converted to cDNA using the RT^2 First strand kit (SABiosciences, Qiagen) and mixed with RT^2 qPCR SYBR Green Mastermix (SABiosciences, Qiagen, Valencia, CA, USA). Samples were loaded and read *via* manufactures' instructions into a 384-well PI3K-AKT signaling PCR array (SABiosciences, Valencia, CA, USA) on a Roche Light Cycler 480. The melt curves and threshold cycle values were determined utilizing the Roche Light Cycler program. The 84 genes that were assessed in the array were related to the PI3K-AKT signaling pathway, after analysis utilizing RT^2 Profiler PCR Array data analysis software (http://pcrdataanalysis.sabiosciences.com/pcr/arrayanalysis.php, SABiosciences, Qiagen, Valencia,

CA, USA). Following the array data analysis software investigation and identification, the genes that were regulated were processed utilizing online data mining software tools, by GATHER,[42] to provide information on other pathway regulations.

Statistical Analysis. All experiments were performed in triplicate, and the results were presented as mean ± standard deviation. Student's *t* test (two tailed, unpaired) was performed for samples of nanoparticle-treated cells *vs* controls, unless stated otherwise. The difference between values was considered significant at the level of $p < 0.05$.

Conflict of Interest: The authors declare no competing financial interest.

Acknowledgment. We would like to thank Dr. Chris Rodesh and Nancy Chandler from the University of Utah Core Facilities for help with confocal microscopy and TEM imaging, respectively. This research was supported by a predoctoral Whitaker Foundation fellowship, Department of Defense Breast Cancer predoctoral fellowship (W81XWH-11-1-0057), National Institutes of Health (R01-DE19050), the Utah Science Technology and Research (USTAR) Initiative, and the Helmholtz Institute for Pharmaceutical Research Saarland (HIPS), Germany.

Supporting Information Available: Physicochemical characterization and TEM images of silica nanomaterials, confocal images of silica nanoparticles in immortalized and primary cells, viability data, time-dependent uptake data, energy-dependent mechanism data, inhibitor cell viability data, wortmannin data, and GATHER analysis. This material is available free of charge *via* the Internet at http://pubs.acs.org.

REFERENCES AND NOTES

1. Nel, A. E.; Madler, L.; Velegol, D.; Xia, T.; Hoek, E. M.; Somasundaran, P.; Klaessig, F.; Castranova, V.; Thompson, M. Understanding Biophysicochemical Interactions at the Nano-Bio Interface. *Nat. Mater.* **2009**, *8*, 543–557.
2. Jones, A. T.; Gumbleton, M.; Duncan, R. Understanding Endocytic Pathways and Intracellular Trafficking: A Prerequisite for Effective Design of Advanced Drug Delivery Systems. *Adv. Drug Delivery Rev.* **2003**, *55*, 1353–1357.
3. Wang, L. H.; Rothberg, K. G.; Anderson, R. G. Mis-Assembly of Clathrin Lattices on Endosomes Reveals a Regulatory Switch for Coated Pit Formation. *J. Cell Biol.* **1993**, *123*, 1107–1117.
4. Pelkmans, L.; Burli, T.; Zerial, M.; Helenius, A. Caveolin-Stabilized Membrane Domains as Multifunctional Transport and Sorting Devices in Endocytic Membrane Traffic. *Cell* **2004**, *118*, 767–780.
5. Wiewrodt, R.; Thomas, A. P.; Cipelletti, L.; Christofidou-Solomidou, M.; Weitz, D. A.; Feinstein, S. I.; Schaffer, D.; Albelda, S. M.; Koval, M.; Muzykantov, V. R. Size-Dependent Intracellular Immunotargeting of Therapeutic Cargoes into Endothelial Cells. *Blood* **2002**, *99*, 912–922.
6. Muro, S.; Garnacho, C.; Champion, J. A.; Leferovich, J.; Gajewski, C.; Schuchman, E. H.; Mitragotri, S.; Muzykantov, V. R. Control of Endothelial Targeting and Intracellular Delivery of Therapeutic Enzymes by Modulating the Size and Shape of Icam-1-Targeted Carriers. *Mol. Ther.* **2008**, *16*, 1450–1458.
7. Jones, A. T. Macropinocytosis: Searching for an Endocytic Identity and Role in the Uptake of Cell Penetrating Peptides. *J. Cell Mol. Med.* **2007**, *11*, 670–684.
8. Champion, J. A.; Mitragotri, S. Shape Induced Inhibition of Phagocytosis of Polymer Particles. *Pharm. Res.* **2009**, *26*, 244–249.
9. Hong, S.; Bielinska, A. U.; Mecke, A.; Keszler, B.; Beals, J. L.; Shi, X.; Balogh, L.; Orr, B. G.; Baker, J. R., Jr.; Banaszak Holl, M. M. Interaction of Poly(Amidoamine) Dendrimers with Supported Lipid Bilayers and Cells: Hole Formation and the Relation to Transport. *Bioconjugate Chem.* **2004**, *15*, 774–782.
10. Doshi, N.; Mitragotri, S. Needle-Shaped Polymeric Particles Induce Transient Disruption of Cell Membranes. *J. R. Soc., Interface* **2010**, *7*, S403–S410.
11. Vercauteren, D.; Vandenbroucke, R. E.; Jones, A. T.; Rejman, J.; Demeester, J.; De Smedt, S. C.; Sanders, N. N.; Braeckmans, K. The Use of Inhibitors to Study Endocytic Pathways of Gene Carriers: Optimization and Pitfalls. *Mol. Ther.* **2010**, *18*, 561–569.
12. Meng, H.; Yang, S.; Li, Z.; Xia, T.; Chen, J.; Ji, Z.; Zhang, H.; Wang, X.; Lin, S.; Huang, C.; *et al*. Aspect Ratio Determines the Quantity of Mesoporous Silica Nanoparticle Uptake by a Small Gtpase-Dependent Macropinocytosis Mechanism. *ACS Nano* **2011**, *5*, 4434–4447.
13. Decuzzi, P.; Ferrari, M. The Role of Specific and Non-Specific Interactions in Receptor-Mediated Endocytosis of Nanoparticles. *Biomaterials* **2007**, *28*, 2915–2922.
14. Decuzzi, P.; Ferrari, M. The Receptor-Mediated Endocytosis of Nonspherical Particles. *Biophys. J.* **2008**, *94*, 3790–3797.
15. Rejman, J.; Oberle, V.; Zuhorn, I. S.; Hoekstra, D. Size-Dependent Internalization of Particles *via* the Pathways of Clathrin- and Caveolae-Mediated Endocytosis. *Biochem. J.* **2004**, *377*, 159–169.
16. Rivera-Gil, P.; Jimenez De Aberasturi, D.; Wulf, V.; Pelaz, B.; Del Pino, P.; Zhao, Y.; De La Fuente, J. M.; Ruiz De Larramendi, I.; Rojo, T.; Liang, X. J.; *et al*. The Challenge to Relate the Physicochemical Properties of Colloidal Nanoparticles to Their Cytotoxicity. *Acc. Chem. Res.* **2012**.
17. Moros, M.; Hernaez, B.; Garet, E.; Dias, J. T.; Saez, B.; Grazu, V.; Gonzalez-Fernandez, A.; Alonso, C.; de la Fuente, J. M. Monosaccharides *versus* PEG-Functionalized NPs: Influence in the Cellular Uptake. *ACS Nano* **2012**, *6*, 1565–1577.
18. Chithrani, B. D.; Chan, W. C. W. Elucidating the Mechanism of Cellular Uptake and Removal of Protein-Coated Gold Nanoparticles of Different Sizes and Shapes. *Nano Lett.* **2007**, *7*, 1542–1550.
19. Gratton, S. E. A.; Napier, M. E.; Ropp, P. A.; Tian, S.; DeSimone, J. M. Microfabricated Particles for Engineered Drug Therapies: Elucidation into the Mechanisms of Cellular Internalization of Print Particles. *Pharm. Res.* **2008**, *25*, 2845–2852.
20. Gratton, S. E. A.; Ropp, P. A.; Pohlhaus, P. D.; Luft, J. C.; Madden, V. J.; Napier, M. E.; DeSimone, J. M. The Effect of Particle Design on Cellular Internalization Pathways. *Proc. Natl. Acad. Sci.* **2008**, *105*, 11613–11618.
21. Albanese, A.; Sykes, E. A.; Chan, W. C. W. Rough around the Edges: The Inflammatory Response of Microglial Cells to Spiky Nanoparticles. *ACS Nano* **2010**, *4*, 2490–2493.
22. Chithrani, B. D.; Ghazani, A. A.; Chan, W. C. W. Determining the Size and Shape Dependence of Gold Nanoparticle Uptake into Mammalian Cells. *Nano Lett.* **2006**, *6*, 662–668.
23. Doshi, N.; Mitragotri, S. Macrophages Recognize Size and Shape of Their Targets. *PLoS One* **2010**, *5*, e10051.
24. Yoo, J. W.; Doshi, N.; Mitragotri, S. Endocytosis and Intracellular Distribution of PLGA Particles in Endothelial Cells: Effect of Particle Geometry. *Macromol. Rapid Commun.* **2009**, *31*, 142–148.
25. Herd, H. L.; Malugin, A.; Ghandehari, H. Silica Nanoconstruct Cellular Toleration Threshold *in Vitro*. *J. Controlled Release* **2011**, *153*, 40–48.
26. Malugin, A.; Herd, H.; Ghandehari, H. Differential Toxicity of Amorphous Silica Nanoparticles toward Phagocytic and Epithelial Cells. *J. Nanopart. Res.* **2011**, *13*, 5381–5396.
27. Parton, R. G.; Richards, A. A. Lipid Rafts and Caveolae as Portals for Endocytosis: New Insights and Common Mechanisms. *Traffic* **2003**, *4*, 724–738.
28. Pohlmann, R.; Kruger, S.; Hasilik, A.; von Figura, K. Effect of Monensin on Intracellular Transport and Receptor-Mediated Endocytosis of Lysosomal Enzymes. *Biochem. J.* **1984**, *217*, 649–658.
29. Kumari, S.; Mg, S.; Mayor, S. Endocytosis Unplugged: Multiple Ways to Enter the Cell. *Cell Res.* **2010**, *20*, 256–275.
30. Gargalovic, P.; Dory, L. Caveolin-1 and Caveolin-2 Expression in Mouse Macrophages. High Density Lipoprotein 3-Stimulated Secretion and a Lack of Significant Subcellular Co-Localization. *J. Biol. Chem.* **2001**, *276*, 26164–26170.
31. Xu, Y.; Krause, A.; Hamai, H.; Harvey, B. G.; Worgall, T. S.; Worgall, S. Proinflammatory Phenotype and Increased

Caveolin-1 in Alveolar Macrophages with Silenced CFTR mRNA. *PLoS One* **2010**, *5*, e11004.
32. Khalil, I. A.; Kogure, K.; Akita, H.; Harashima, H. Uptake Pathways and Subsequent Intracellular Trafficking in Nonviral Gene Delivery. *Pharmacol. Rev.* **2006**, *58*, 32–45.
33. Piasek, A.; Thyberg, J. Effects of Colchicine on Endocytosis of Horseradish Peroxidase by Rat Peritoneal Macrophages. *J Cell Sci.* **1980**, *45*, 59–71.
34. Piasek, A.; Oblakowski, P. Influence of Colchicine and Cytochalasin B on Pinocytosis, Phagocytosis, and Antibody-Dependent Cell-Mediated Cytotoxicity. *Haematol. Blood Transfus.* **1985**, *29*, 511–513.
35. Valberg, P. A.; Brain, J. D.; Kane, D. Effects of Colchicine or Cytochalasin B on Pulmonary Macrophage Endocytosis *in Vivo*. *J. Appl. Physiol.* **1981**, *50*, 621–629.
36. Davies, P. J.; Cornwell, M. M.; Johnson, J. D.; Reggianni, A.; Myers, M.; Murtaugh, M. P. Studies on the Effects of Dansylcadaverine and Related Compounds on Receptor-Mediated Endocytosis in Cultured Cells. *Diabetes Care* **1984**, *7*), 35–41.
37. Cox, D.; Tseng, C. C.; Bjekic, G.; Greenberg, S. A Requirement for Phosphatidylinositol 3-Kinase in Pseudopod Extension. *J. Biol. Chem.* **1999**, *274*, 1240–1247.
38. Araki, N.; Johnson, M. T.; Swanson, J. A. A Role for Phosphoinositide 3-Kinase in the Completion of Macropinocytosis and Phagocytosis by Macrophages. *J. Cell Biol.* **1996**, *135*, 1249–1260.
39. Doherty, G. J.; McMahon, H. T. Mechanisms of Endocytosis. *Annu. Rev. Biochem.* **2009**, *78*, 857–902.
40. Champion, J. A.; Walker, A.; Mitragotri, S. Role of Particle Size in Phagocytosis of Polymeric Microspheres. *Pharm. Res.* **2008**, *25*, 1815–1821.
41. Vacha, R.; Martinez-Veracoechea, F. J.; Frenkel, D. Receptor-Mediated Endocytosis of Nanoparticles of Various Shapes. *Nano Lett.* **2011**, *11*, 5391–5395.
42. Chang, J. T.; Nevins, J. R. Gather: A Systems Approach to Interpreting Genomic Signatures. *Bioinformatics* **2006**, *22*, 2926–2933.
43. Yamamoto, A.; Cremona, M. L.; Rothman, J. E. Autophagy-Mediated Clearance of Huntingtin Aggregates Triggered by the Insulin-Signaling Pathway. *J. Cell Biol.* **2006**, *172*, 719–731.
44. Chang, Y. Y.; Juhasz, G.; Goraksha-Hicks, P.; Arsham, A. M.; Mallin, D. R.; Muller, L. K.; Neufeld, T. P. Nutrient-Dependent Regulation of Autophagy through the Target of Rapamycin Pathway. *Biochem. Soc. Trans.* **2009**, *37*, 232–236.
45. Armour, S. M.; Baur, J. A.; Hsieh, S. N.; Land-Bracha, A.; Thomas, S. M.; Sinclair, D. A. Inhibition of Mammalian S6 Kinase by Resveratrol Suppresses Autophagy. *Aging (Albany NY)* **2009**, *1*, 515–528.
46. Huh, S.; Wiench, J. W.; Yoo, J. C.; Pruski, M.; Lin, V. Organic Functionalization and Morphology Control of Mesoporous Silicas *via* a Co-Condensation Synthesis Method. *Chem. Mater.* **2003**, *15*, 4247–4256.
47. Blaaderen, A.; Vrji, A. Synthesis and Characterization of Colloidal Dispersions of Fluorescent Silica Spheres. *Langmuir* **1992**, *8*, 2921–2931.
48. Daum, N.; Kuehn, A.; Hein, S.; Schaefer, U. F.; Huwer, H.; CM., L. Isolation, Cultivation, and Application of Human Alveolar Epithelial Cells. *Methods Mol. Biol.* **2012**, *806*, 31–42.
49. Hoppstadter, J.; Diesel, B.; Zarbock, R.; Breinig, T.; Monz, D.; Koch, M.; Meyerhans, A.; Gortner, L.; Lehr, C. M.; Huwer, H.; *et al*. Differential Cell Reaction Upon Toll-Like Receptor 4 and 9 Activation in Human Alveolar and Lung Interstitial Macrophages. *Respir. Res.* **2010**, *11*, 124.
50. Zaki, N. M.; Tirelli, N. Gateways for the Intracellular Access of Nanocarriers: A Review of Receptor-Mediated Endocytosis Mechanisms and of Strategies in Receptor Targeting. *Expert Opin. Drug Delivery* **2010**, *7*, 895–913.
51. Feng, S.-z.; Cao, W.-s.; Liao, M. The PI3K/Akt Pathway Is Involved in Early Infection of Some Exogenous Avian Leukosis Viruses. *J. Gen. Virol.* **2011**, *92*, 1688–1697.